Available online at www.sciencedirect.com
ScienceDirect
International Journal of Heat and Mass Transfer 51 (2008) 4691–4703
International Journal of HEAT and MASS TRANSFER
www.elsevier.com/locate/ijhmt

Natural convection in a heat generating hydrodynamically and thermally anisotropic non-Darcy porous medium

D. Jaya Krishna [a], Tanmay Basak [b], Sarit K. Das [a,*]

[a] Heat Transfer and Thermal Power Laboratory, Department of Mechanical Engineering, Indian Institute of Technology Madras, Chennai 600 036, India
[b] Department of Chemical Engineering, Indian Institute of Technology Madras, Chennai 600 036, India

Received 8 November 2007; received in revised form 16 February 2008
Available online 10 April 2008

Abstract

Natural convection in a two-dimensional square cavity containing hydrodynamically and thermally anisotropic porous medium with internal heat generation is analyzed numerically by generalized non-Darcy approach. The properties considered for the study are permeability ratio (K^*), inclination of the principal axes (θ), ratio of Forchheimer constants (F^*) and thermal conductivity ratio (k^*). Results are presented in terms of isotherms, streamlines and maximum temperature in the cavity to understand the flow physics. It is observed that the anisotropic properties have significant influence on the flow behaviour and heat transfer. A correlation for maximum temperature in the cavity for a wide range of parameters ($10^7 \leqslant Ra \leqslant 10^8$, $10^{-6} \leqslant Da \leqslant 10^{-3}$, $0° \leqslant \theta \leqslant 90°$, $1 \leqslant F^* \leqslant 100$, $0.1 \leqslant K^* \leqslant 10$ and $0.1 \leqslant k^* \leqslant 10$) is developed.

Keywords: Natural convection; Generalized non-Darcy approach; Anisotropic porous medium; Heat generation

1. Introduction

Natural convection in fluid saturated heat generating porous media has several applications in engineering and nature. Such applications include exothermic reactions in packed bed reactors, heat transfer associated with the deep storage of nuclear waste, flow past heat exchanger tubes and to study the effect of the metabolic heat generation in grains causing hot spots that induce fungal growth [1–3]. However, in many applications, porous materials are anisotropic due to preferential orientation for drying of food grains, rod bundles in a nuclear reactor core and heat exchanger tubes etc. A detailed analysis on natural convection in a heat generating anisotropic porous medium is yet to appear in the literature.

The earlier studies of natural convection in enclosures filled with volumetrically heated isotropic Darcy porous medium are due to Beukema et al. [4], Haajizadeh et al. [5] and Prasad [1]. Royer and Flores [6] numerically examined natural convection in a rectangular enclosure filled with heat generating anisotropic and heterogeneous Darcy porous medium. Suresh et al. [7] carried out numerical simulation of 3D natural convection inside a heat generating anisotropic porous medium by Darcy approach. The deviation of Darcy formulation for coarsely packed porous media led to generalized non-Darcy formulation [8–11]. Flow behavior and heat transfer aspects of a heat generating isotropic porous media has been numerically investigated by Anwar and Wilson [12] with non-Darcy approach for non isothermal walls, and Jue [13] with generalized non-Darcy approach for a differentially heated cavity. However, most of the porous materials are anisotropic due to preferential orientation for either enhancing

* Corresponding author. Present address: Department of Mechanical Engineering, Massachusetts Institute of Technology, 77 Massachusetts Avenue, Room 3-354A, Cambridge, MA 02139-4307, USA. Tel.: +91 44 2257 4655; fax: +91 44 2257 4652.
E-mail address: skdas@iitm.ac.in (S.K. Das).

0017-9310/$ - see front matter © 2008 Elsevier Ltd. All rights reserved.
doi:10.1016/j.ijheatmasstransfer.2008.02.019

Nomenclature

C	Forchheimer coefficient (m^{-1}) (Eqs. (9), (10), (14))
C^*	ratio of Forchheimer coefficients (Eq. (12))
C_p	specific heat ($J\ kg^{-1}\ K^{-1}$)
Da	Darcy number (Eq. (18))
F	Forchheimer constant
F^*	ratio of Forchheimer constants (Eq. (11))
g	acceleration due to gravity ($m\ s^{-2}$)
K	permeability (m^2)
k	thermal conductivity ($W\ m^{-1}\ K^{-1}$) (Eq. (5))
K^*	permeability ratio (Eq. (8))
k^*	thermal conductivity ratio (Eq. (16))
L	cavity width (characteristic dimension) (m)
$\overline{Nu}$	average Nusselt number (Eqs. (25)–(27))
P	pressure ($N\ m^{-2}$)
Pr	Prandtl number
Q	non-dimensional heat generation (Eq. (18))
q''	uniform heat flux ($W\ m^{-2}$)
q'''_v	volumetric heat generation ($W\ m^{-3}$)
Ra	Rayleigh number (Eq. (18))
Ra_I	internal Rayleigh number for case 3
Ra_m	Rayleigh Darcy number ($=Ra \cdot Da$)
T	temperature (K/non dimensional temperature)
t	time (s)
T_{mean}	non dimensional mean temperature on the line of symmetry
u	volume averaged velocity in x-direction ($m\ s^{-1}$)
v	volume averaged velocity in y-direction ($m\ s^{-1}$)
$\lvert V\rvert$	magnitude of velocity vector $\left(\sqrt{u^2+v^2}\right)$ (m)
x, y	coordinates axes

Greek symbols

ϕ	T_m or $\overline{Nu}$
ψ	stream function
ζ	u, v or T variable
ρ	density ($kg\ m^{-3}$)
ν	kinematic viscosity ($m^2\ s^{-1}$)
μ	viscosity of fluid ($N\ s\ m^{-2}$)
β	coefficient of thermal expansion (K^{-1})
ε	porosity (void volume/total volume)
θ	inclination of principal axes, degrees
σ	ratio of heat capacities (Eq. (4))

Subscripts

1,2	direction of principal axes
c	cold
f	fluid
h	hot
m	maximum
p	porous medium
so	solid matrix

Superscripts

$*$	ratio of anisotropic properties
$'$	non-dimensional quantities
$=$	tensor
i, $i-1$	present and previous grid size
n, $n-1$	present and previous time step

or for deteriorating heat transfer. Considering its importance Degan and co-investigators [14–16] and Nithiarasu et al. [3] numerically investigated natural convection in a fluid saturated porous medium which is assumed to be hydrodynamically anisotropic with its principal axes oriented in a direction that is oblique to the gravity vector. They found that the orientation of principal axes and permeability ratio have significant influence on the flow behaviour and heat transfer. In the above-mentioned paper [3] the Forchheimer constant has been considered constant. Nakayama et al. [17,18] numerically studied fluid flow and heat transfer through an anisotropic porous medium and demonstrated the function of macroscopic flow angle on directional Forchheimer coefficient. As the Forchheimer coefficient is defined as the ratio of Forchheimer constant to the square root of permeability (Eq. (10)), there arises a question whether the variation of Forchheimer constant is also to be considered with respect to direction. Till date, a comprehensive study on natural convection in a heat generating anisotropic porous medium with a proposed correlation for maximum temperature in the non-Darcy regime is yet to appear in the literature. Also, the natural convection in a non-Darcy heat generating anisotropic porous medium requires extensive investigation due to its wide range of applications.

The present study is a first attempt to analyze natural convection inside a square cavity filled with heat generating porous medium which is assumed to be hydrodynamically and thermally anisotropic in nature. Hydrodynamic anisotropy is based on both permeability and Forchheimer coefficient which are arbitrary oriented with respect to gravity. Also, the thermal conductivity is assumed to vary orthotropic with respect to gravity vector. The following range of parameters such as Rayleigh number ($10^7 \leqslant Ra \leqslant 10^8$), Darcy number ($10^{-6} \leqslant Da \leqslant 10^{-3}$), inclination of principal axes ($0° \leqslant \theta \leqslant 90°$), ratio of Forchheimer constants ($1 \leqslant F^* \leqslant 100$), permeability ratio ($0.1 \leqslant K^* \leqslant 10$) and thermal conductivity ratio ($0.1 \leqslant k^* \leqslant 10$) have been considered with a porosity of 0.8 to understand the influence of anisotropic properties on flow behavior and heat transfer and also, to generate correlation for maximum temperature in the cavity for a heat generating anisotropic porous medium.

Several practical applications can be indicated for the above mentioned range of parameters. One of the examples can be heat generating rod bundle for nuclear application,

which can be analyzed as a heat generating anisotropic porous medium. Considering rod diameter (0.008 m) and heat generation (50 W/heater) from Suresh et al. [7] and taking correlations for the permeability in x-direction, permeability ratio and thermal conductivity ratio from Lee and Yang [19,20], the following parameters are obtained. For $\theta = 0°$ with $k_s/k_f = 27.18$ (carbon steel) and $\varepsilon = 0.8$: $Ra = 4.74 \times 10^7$, $K_x = 5.01 \times 10^{-6}\,\mathrm{m}^2$, $K^* = 0.497$ and $k^* = 0.224$. Based on the reference length (i.e. width of the cavity) the Darcy number can be varied from 10^{-3} to 10^{-6} (e.g. $L = 0.075$ m, $Da = 8.91 \times 10^{-4}$).

Based on the above observations, the objectives of the present work are chosen (i) to analyze the influence of anisotropic properties on the flow behaviour and heat transfer and (ii) to obtain a correlation for the maximum temperature in the cavity for heat generating anisotropic porous medium with specified range of parameters.

2. Mathematical formulation

The schematic diagram of a two dimensional square porous cavity with vertical walls isothermally cooled and adiabatic horizontal sides is shown in Fig. 1. The cavity is filled with fluid saturated anisotropic porous medium which generate heat at a uniform rate. It is assumed that the solid matrix of the porous media does not undergo deformation and is anisotropic in permeability, Forchheimer coefficient and thermal conductivity. The fluid is considered to be in local thermal equilibrium with the solid matrix. Density variation of the fluid follows Boussinesq's assumption. Generalized non-Darcy approach has been considered and the governing equations are solved using a pseudo-transient approach. Hence, the equations in terms of primitive variables for transient flow can be written as follows.

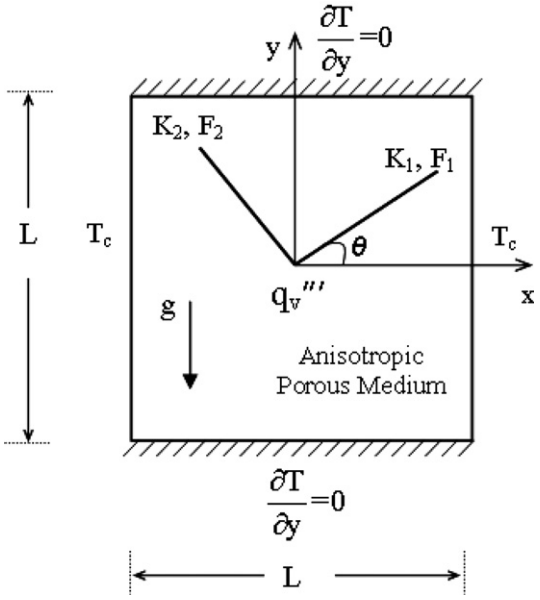

Fig. 1. Problem geometry.

$$\nabla \cdot V = 0, \tag{1}$$

$$\frac{\rho_f}{\varepsilon}\left[\frac{\partial V}{\partial t} + \left(\frac{V}{\varepsilon}\right)\cdot\nabla V\right] = -\nabla P_f + \frac{\mu_f}{\varepsilon}\nabla^2 V - \frac{\mu_f}{\overline{\overline{K}}}V - \overline{\overline{C}}\rho_f V|V| + \rho_f \beta g(T - T_C), \tag{2}$$

$$(\rho C_p)_f\left[\frac{\partial(\sigma T)}{\partial t} + V\cdot\nabla T\right] = \nabla\cdot\left(\bar{\bar{k}}\nabla T\right) + q'''_v, \tag{3}$$

where

$$\sigma = \frac{\varepsilon\rho_f C_{pf} + (1-\varepsilon)\rho_{so}C_{pso}}{\rho_f C_{pf}}, \tag{4}$$

$$k_x = \varepsilon k_f + (1-\varepsilon)k_{so}, \tag{5}$$

$$q'''_v = \varepsilon q'''_f + (1-\varepsilon)q'''_{so}, \tag{6}$$

$$\overline{\overline{K}} = \begin{bmatrix} K_1\cos^2\theta + K_2\sin^2\theta & (K_1-K_2)\sin\theta\cos\theta \\ (K_1-K_2)\sin\theta\cos\theta & K_2\cos^2\theta + K_1\sin^2\theta \end{bmatrix}, \tag{7}$$

$$K^* = \frac{K_1}{K_2}, \tag{8}$$

$$\overline{\overline{C}} = \begin{bmatrix} C_1\cos^2\theta + C_2\sin^2\theta & (C_1-C_2)\sin\theta\cos\theta \\ (C_1-C_2)\sin\theta\cos\theta & C_2\cos^2\theta + C_1\sin^2\theta \end{bmatrix}, \tag{9}$$

$$C_1 = \frac{F_1}{\sqrt{K_1}}, \quad C_2 = \frac{F_2}{\sqrt{K_2}}, \tag{10}$$

$$F^* = \frac{F_1}{F_2}, \tag{11}$$

$$C^* = \frac{C_1}{C_2} = \frac{F^*}{\sqrt{K^*}}. \tag{12}$$

Substituting K^* (Eq. (8)) in Eq. (7) and by applying inverse, the permeability tensor can be reduced to

$$\overline{\overline{K^{-1}}} = \frac{1}{K_1}\begin{bmatrix} \cos^2\theta + K^*\sin^2\theta & (1-K^*)\sin\theta\cos\theta \\ (1-K^*)\sin\theta\cos\theta & K^*\cos^2\theta + \sin^2\theta \end{bmatrix}. \tag{13}$$

Substituting C^* (Eq. (12)) in Eq. (9), the Forchheimer coefficient tensor can be reduced to

$$\overline{\overline{C}} = \frac{F_1}{\sqrt{K_1}}\begin{bmatrix} \cos^2\theta + \frac{\sqrt{K^*}}{F^*}\sin^2\theta & \left(1-\frac{\sqrt{K^*}}{F^*}\right)\sin\theta\cos\theta \\ \left(1-\frac{\sqrt{K^*}}{F^*}\right)\sin\theta\cos\theta & \frac{\sqrt{K^*}}{F^*}\cos^2\theta + \sin^2\theta \end{bmatrix}, \tag{14}$$

$$\bar{\bar{k}} = \begin{bmatrix} k_x & 0 \\ 0 & k_y \end{bmatrix}, \tag{15}$$

$$k^* = \frac{k_y}{k_x}. \tag{16}$$

Substituting k^* (Eq. (16)) in Eq. (15), the thermal conductivity tensor can be reduced to

$$\bar{\bar{k}} = k_x\begin{bmatrix} 1 & 0 \\ 0 & k^* \end{bmatrix}. \tag{17}$$

Using the following dimensionless variables

$$
\begin{aligned}
&x' = \frac{x}{L}, \quad y' = \frac{y}{L}, \quad \alpha_x = \frac{k_x}{(\rho C_p)_f} \\
&u' = \frac{u}{(\alpha_x/L)}, \quad v' = \frac{v}{(\alpha_x/L)}, \quad t' = \frac{t}{(L^2/\alpha_x)}, \\
&Pr = \frac{\nu_f}{\alpha_x}, \quad Da = \frac{K_1}{L^2}, \quad Ra = \frac{g\beta\Delta T L^3}{\nu_f \alpha_x}, \\
&P' = \frac{P_f}{(\rho\alpha_x^2/L^2)}, T' = \frac{T - T_c}{\Delta T}, \quad Q = \frac{q_v''' L^2}{\Delta T k_x}.
\end{aligned} \tag{18}
$$

Note that the prime symbol has been ignored for the sake of convenience and the governing equations in non dimensional form are as follows:

$$\frac{\partial u}{\partial x} + \frac{\partial v}{\partial y} = 0, \tag{19}$$

$$
\begin{aligned}
&\left[\frac{1}{\varepsilon}\frac{\partial u}{\partial t} + \frac{u}{\varepsilon^2}\frac{\partial u}{\partial x} + \frac{v}{\varepsilon^2}\frac{\partial u}{\partial y}\right] = -\frac{\partial P}{\partial x} + \frac{Pr}{\varepsilon}\left(\frac{\partial^2 u}{\partial x^2} + \frac{\partial^2 u}{\partial y^2}\right) \\
&-\frac{Pr}{Da}\left[u\left(\cos^2\theta + K^*\sin^2\theta\right) + v\left((1-K^*)\sin\theta\cos\theta\right)\right] \\
&-\frac{F_1}{\sqrt{Da}}\left[u\left(\cos^2\theta + \frac{\sqrt{K^*}}{F^*}\sin^2\theta\right)\right. \\
&\left.+ v\left(\left(1 - \frac{\sqrt{K^*}}{F^*}\right)\sin\theta\cos\theta\right)\right]\sqrt{u^2+v^2},
\end{aligned} \tag{20}
$$

$$
\begin{aligned}
&\left[\frac{1}{\varepsilon}\frac{\partial v}{\partial t} + \frac{u}{\varepsilon^2}\frac{\partial v}{\partial x} + \frac{v}{\varepsilon^2}\frac{\partial v}{\partial y}\right] = -\frac{\partial P}{\partial y} + \frac{Pr}{\varepsilon}\left(\frac{\partial^2 v}{\partial x^2} + \frac{\partial^2 v}{\partial y^2}\right) \\
&-\frac{Pr}{Da}\left[u\left((1-K^*)\sin\theta\cos\theta\right) + v\left(K^*\cos^2\theta + \sin^2\theta\right)\right] \\
&-\frac{F_1}{\sqrt{Da}}\left[u\left(\left(1 - \frac{\sqrt{K^*}}{F^*}\right)\sin\theta\cos\theta\right)\right. \\
&\left.+ v\left(\frac{\sqrt{K^*}}{F^*}\cos^2\theta + \sin^2\theta\right)\right]\sqrt{u^2+v^2} + Ra\cdot Pr\cdot T,
\end{aligned} \tag{21}
$$

$$\frac{\partial(\sigma T)}{\partial t} + u\frac{\partial T}{\partial x} + v\frac{\partial T}{\partial y} = \frac{\partial^2 T}{\partial x^2} + k^*\frac{\partial^2 T}{\partial y^2} + 1. \tag{22}$$

In the non-dimensional governing equations the Forchheimer constant is taken as $F_1 \approx 0.55$ which was experimentally measured by Ward [21] (also in [22]) and u and v are volume averaged velocity components. The Prandtl number and porosity are taken to be 0.71 and 0.8 throughout the computations.

The following cases have been considered to check the validity of the present formulation and numerical procedure.

Note that, the present parametric study considers Case: 2(a).

Case 1:

(a) Differentially heated condition without volumetric heat generation (Ref. [23])

$$\Delta T = T_h - T_c$$
$$Q = 0.$$

(b) Constant heat flux condition (left and right walls) without volumetric heat generation (Ref. [3,15]).

$$\Delta T = \frac{q'' L}{k_x}, \quad Q = 0.$$

Case 2:

(a) Isothermally cooled side walls (left and right walls) with volumetric heat generation [Present study].

$$\Delta T = \frac{q_v''' L^2}{k_x}, \quad Q = 1 \quad \text{(see Eq. (18))}.$$

(b) Isothermally cooled side walls (left wall symmetry condition and right wall isothermally cooled) with volumetric heat generation for square cavity (Ref. [1]).

$$\Delta T = \frac{q_v''' L^2}{2k_x}, \quad Q = 2 \quad \text{(see Eq. (18))}.$$

Case 3:

Differentially heated porous cavity with volumetric heat generation (Ref. [13])

$$\Delta T = T_h - T_c, \quad Ra_I = \frac{g\beta q_v''' L^5}{\nu_f \alpha_x k_x},$$
$$Q = \frac{Ra_I}{Ra} \quad \text{(see Eq. (18))}.$$

Eqs. (19)–(22) will subject to the following boundary conditions:

Initial and Boundary conditions are as follows

(Note that the present parametric study is considered for Case: 2(a))

Initial conditions

$$t = 0; \quad u, v = 0, \quad T = 0.$$

Boundary conditions

Bottom wall

$$t > 0; \quad u, v = 0, \quad \frac{\partial T}{\partial y} = 0 \quad \text{at } y = 0; \quad 0 < x \leqslant L.$$

Top wall

$$t > 0; \quad u, v = 0, \quad \frac{\partial T}{\partial y} = 0 \quad \text{at } y = L; \quad 0 \leqslant x \leqslant L.$$

Left wall

Case: 1(a), 3

$$t > 0; \quad u, v = 0, \quad T = 1 \quad \text{at } x = 0; \quad 0 \leqslant y \leqslant L.$$

Case: 1(b)

$$t > 0; \quad u, v = 0, \quad \frac{\partial T}{\partial x} = -1 \quad \text{at } x = 0; \quad 0 \leqslant y \leqslant L. \tag{23}$$

Case: 2(a)

$$t > 0; \quad u, v = 0, \quad T = 0 \quad \text{at } x = 0; \quad 0 \leqslant y \leqslant L.$$

Case: 2(b)

$$t > 0; \quad u = 0, \frac{\partial v}{\partial x} = 0, \quad \frac{\partial T}{\partial x} = 0 \quad \text{at } x = 0; \quad 0 \leqslant y \leqslant L.$$

Right wall

Case: 1(b)

$$t > 0; \quad u, v = 0, \quad \frac{\partial T}{\partial x} = -1 \quad \text{at } x = L; \quad 0 \leqslant y \leqslant L.$$

Case: 1(a), 2(a,b), 3

$$t > 0; \quad u, v = 0, \quad T = 0 \quad \text{at } x = L; \quad 0 \leqslant y \leqslant L.$$

The fluid motion has been displayed in terms of streamlines. The following relationships between the velocity components (u and v) and stream function (ψ) have been used

$$v = -\frac{\partial \psi}{\partial x}, \quad u = \frac{\partial \psi}{\partial y}. \tag{24}$$

The average Nusselt number is defined by

Case: 1(a), 3

$$\overline{Nu} = -\int_0^1 \left(\frac{\partial T}{\partial x}\right)_{x=0,1} \mathrm{d}y. \tag{25}$$

Case: 2(b)

$$\overline{Nu} = \frac{2}{T_{\text{mean}}}. \tag{26}$$

T_{mean} is the mean temperature on the line of symmetry

Case: 1(b)

$$\overline{Nu} = \frac{1}{\Delta T}. \tag{27}$$

ΔT is the temperature difference between the mid height nodes at the vertical walls.

It is to be noted that the average Nusselt number is not provided for the present study [Case: 2(a)] as the flow behavior and heat transfer aspects are carried out in terms of maximum temperature (T_{m}), isotherms and streamlines. It is observed in literature [1,13] that the average Nusselt number has been reported in different forms for heat generating porous media. The authors believe that, understanding the flow physics in terms of maximum temperature (T_{m}) is more convenient when compared to average Nusselt number. The above mentioned average Nusselt numbers have been employed only for the validation of the present formulation with the literature [1,3,13,15,23].

3. Numerical procedure

The governing equations have been discretized by using finite volume method. Quadrilateral cells in a semi-staggered arrangement introduced by Hirt et al. [24] have been employed. Velocity nodes are located at the vertices and pressure nodes are located at the centroid of the quadrilateral cells. First order upwind scheme is used for convective term formulation. Non-uniform cosine grid has been employed.

For pressure and velocity coupling, the SIMPLE algorithm is used. The momentum equations are solved by Gauss-Seidel point by point iteration method. The iteration process is continued until the following convergence criterion is achieved.

$$\frac{\sum_{i,j}\left|\zeta_{i,j}^{n} - \zeta_{i,j}^{n-1}\right|}{\sum_{i,j}\left|\zeta_{i,j}^{n}\right|} < 10^{-8}, \tag{28}$$

where ζ represents u, v or T variables, n represents present time step, $n-1$ represents previous time step.

4. Grid independence and validation

In order to validate the predictive capability and accuracy of the present porous medium code, computations are performed with various configurations and boundary conditions. The results thus obtained are compared with the available literature [1,3,13,23] wherever possible.

To ensure that the results obtained by the numerical study are independent of the computational grid, grid independence studies are carried out using Eq. (29) between two consecutive grids for the average Nusselt number

Table 2
Comparison of present results for thermally anisotropic porous medium Case: 1(a) ($\theta = 0°$, $K^* = 1$, $F^* = 1$, $\varepsilon = 0.9$ and $Pr = 1$)

S.No.	Ra	Da	k^*	Average Nusselt number	
				Present	Ni and Beckermann [23]
1	10^8	10^{-6}	0.1	3.645	3.721
2	10^8	10^{-6}	1	3.070	3.102
3	10^8	10^{-6}	10	1.871	1.842
4	10^9	10^{-6}	0.1	13.849	14.297
5	10^9	10^{-6}	1	13.040	13.461
6	10^9	10^{-6}	10	9.436	9.851

Table 1
Comparison of present results for anisotropic porous medium Case: 1(b) ($Ra_{\text{m}} = 500$, $k^* = 1$, $\varepsilon = 0.6$ and $Pr = 1$)

S. No	Ra	Da	θ	K^*	Average Nusselt number			$T_{\max} = -T_{\min}$		
					Present	Degan and Vasseur [15]	Nithiarasu et al. [3]	Present	Degan and Vasseur [15]	Nithiarasu et al. [3]
1	5×10^7	10^{-5}	90	10^{-3}	5.652	5.909	5.660	0.241	0.247	0.248
2	5×10^5	10^{-3}	90	10^{-3}	4.489	4.727	4.560	0.295	0.305	0.305
3	5×10^7	10^{-5}	45	10^{2}	1.122	1.173	1.174	0.547	0.576	0.569
4	5×10^5	10^{-3}	45	10^{2}	1.121	1.170	1.170	0.547	0.576	0.570
5	5×10^7	10^{-5}	0	10^{-2}	9.452	10.781	9.950	0.245	0.261	0.236
6	5×10^5	10^{-3}	0	10^{-2}	5.064	5.414	4.729	0.293	0.304	0.314

and maximum temperature in the cavity. For our computations, non uniform cosine grid is employed. It is important to note that the number of iteration steps required satisfying the convergence criteria increases with the increase in mesh size and this practice always ensures a balance of convergence and computational time. It is found that the percentage deviation between 61×61 and 81×81 is less than 1%. Therefore a grid size of 61×61 with the first node from the wall at a non dimensional distance of 0.000685 is considered for computations.

Table 3
Comparison of present results for heat generating porous medium ($\theta = 0°$, $K^* = 1$, $F^* = 1$ and $k^* = 1$)

S.No.	Differentially heated walls ($\varepsilon = 0.4$, $Pr = 0.71$)	Da	Ra	Ra_1	Average Nusselt number	
					Present	Jue [13]
(a)						
1	Case 3	10^{-2}	10^7	10^7	10.91	10.75
2	Case 3	10^{-2}	10^5	10^8	−490.56	−485.60
3	Case 3	10^{-4}	10^6	10^7	−1.836	−1.789
4	Case 3	10^{-4}	10^5	10^7	−46.84	−46.37
5	Case 3	10^{-6}	10^5	10^3	0.995	0.995
6	Case 3	10^{-6}	10^7	10^7	0.607	0.581

S.No.	Isothermally cooled side walls ($\varepsilon = 0.9$, $Pr = 1$)	Da	Ra	Present	Prasad [1]
(b)					
1	Case 2(b)	10^{-6}	10^7	2.190	2.170
2	Case 2(b)	10^{-6}	10^8	4.281	4.350

$$\% \text{ Error} = \left(\frac{\varphi^i - \varphi^{i-1}}{\varphi^i}\right) \times 100, \tag{29}$$

where φ represents T_m or $\overline{Nu}$, i represents present grid size, $i-1$ represents previous grid size.

The formulation for permeability tensor based on earlier literature [3,15] has been considered by taking permeability K_1 with angle θ to vertical axis. In the present study for the sake of convenience, the permeability tensor has been formulated by taking permeability K_1 with angle θ to horizontal axis (x-axis). Therefore, the angle 'θ' in the current study differs by 90° from the values reported in literature. For the validation of natural convective flow in anisotropic porous medium without heat generation for wide range of permeability ratios, a problem with constant heat flux boundary condition at the vertical walls has been considered. In this study, the results are compared with Nithiarasu et al. [3] and Degan and Vasseur [15] by neglecting Forchheimer term and comparison is shown in Table 1.

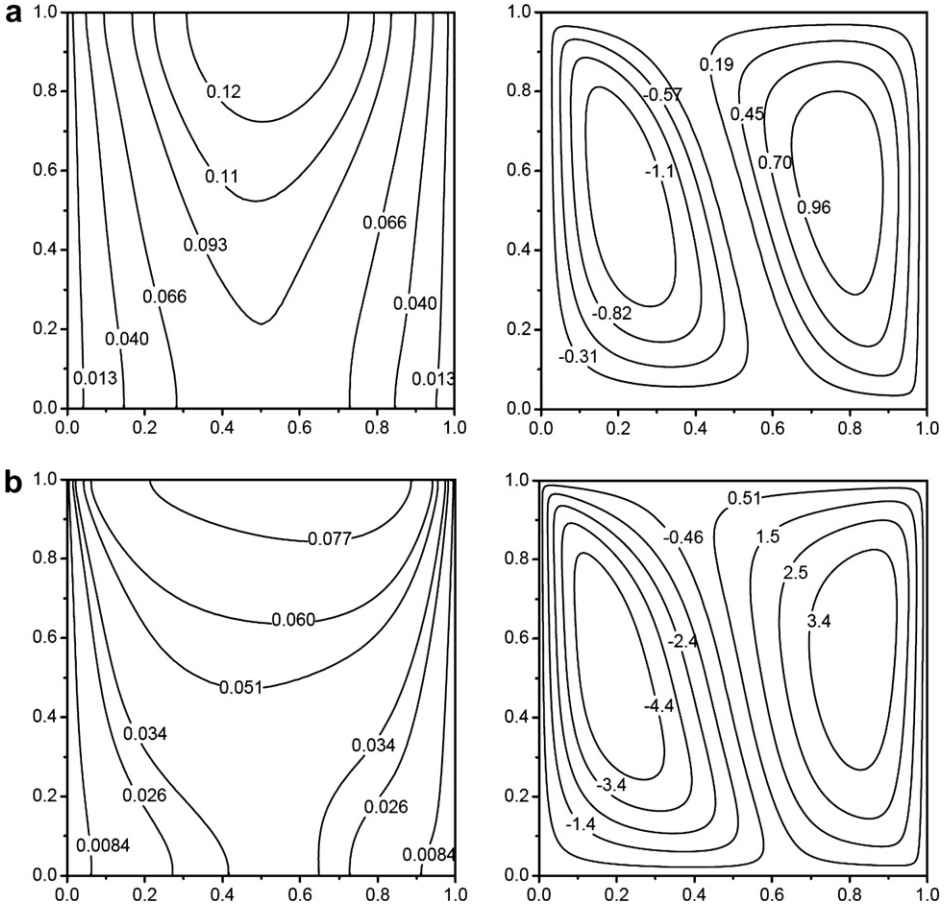

Fig. 2. Isotherms (left) and streamlines (right) for $Da = 10^{-5}$, $K^* = 0.1$, $F^* = 10$, $\theta = 45°$ and $k^* = 1$ with the variation of Rayleigh number (Ra): (a) $Ra = 10^7$ ($T_m = 0.133$); (b) $Ra = 10^8$ ($T_m = 0.086$).

For the validation of thermally anisotropic behavior of the porous medium the results are compared with an earlier work [23] and are shown in Table 2. Table 3a provides comparison between current results and an earlier work [13] for a heat generating differentially heated porous cavity and Table 3b compares current result with the earlier work [1] for a heat generating isothermally cooled side walls. Tables 1–3a,b clearly illustrates that the code has been rigorously validated and the test results agree very well with the literature.

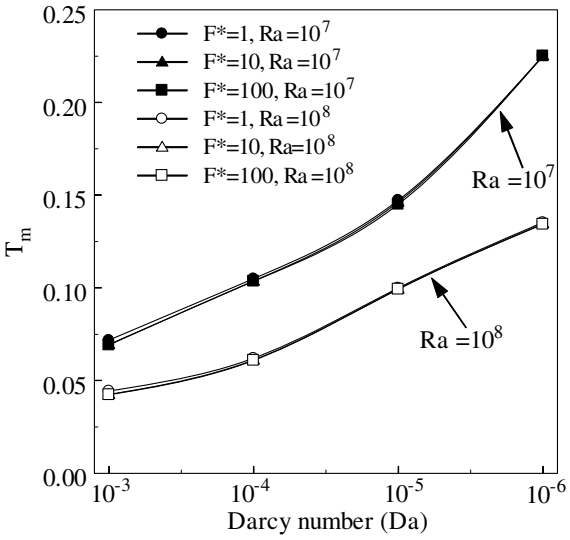

Fig. 3. Effect of ratio of Forchheimer constants (F^*) on the maximum temperature (T_m) with the variation of Darcy number and Rayleigh number for $K^* = 1$, $\theta = 45°$ and $k^* = 1$.

5. Results and discussion

This section demonstrates the influence of Rayleigh number (Ra), Darcy number (Da), permeability ratio (K^*), inclination of principal axes (θ), ratio of Forchheimer constants (F^*) and thermal conductivity ratio (k^*) on the flow behaviour and heat transfer. In this study, the permeability K_1 is assumed to be constant, as Darcy number is defined in terms of K_1 and the permeability K_2 is varied by K^* (Eqs. (8), (18)). The section is divided into two parts, the first part deals with the influence of parameters on the flow behaviour and heat transfer. The second part deals with the correlation for maximum temperature in the cavity in non-Darcy regime. Various results have been analyzed in terms of streamlines, isotherms and maximum temperature (T_m) in the cavity.

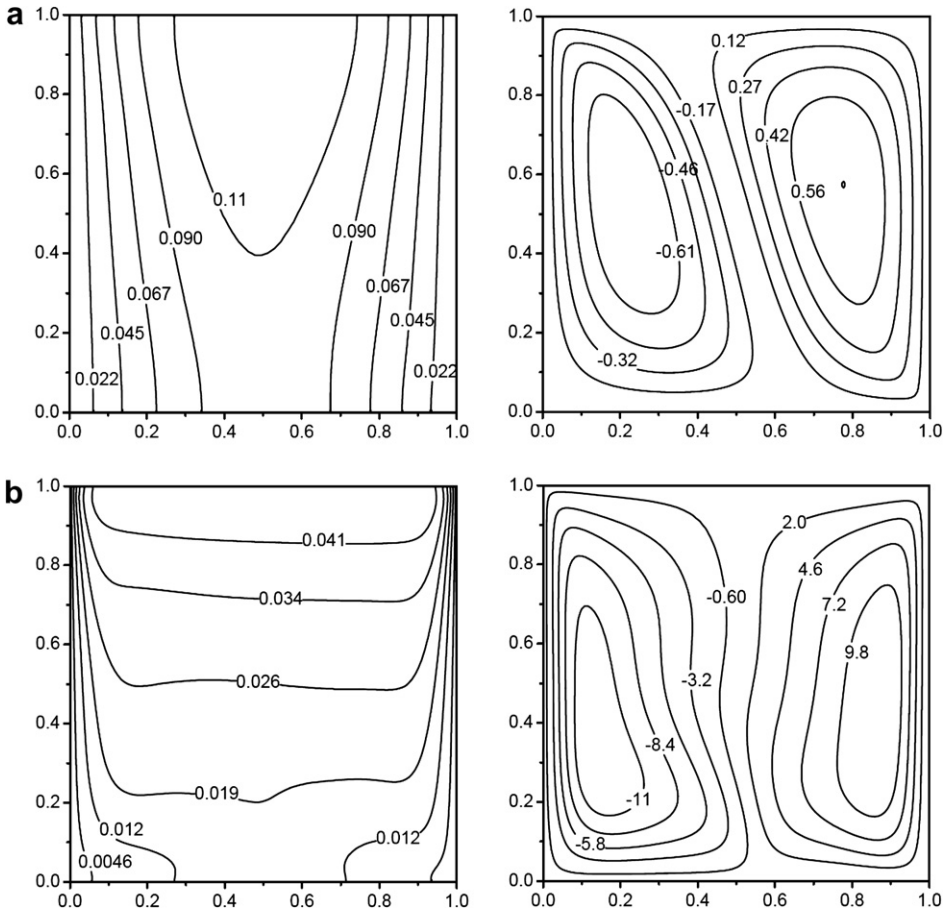

Fig. 4. Isotherms (left) and streamlines (right) for $Ra = 5 \times 10^7$, $K^* = 0.1$, $F^* = 10$, $\theta = 45°$ and $k^* = 1$ with the variation of Darcy number (Da): (a) $Da = 10^{-6}$ ($T_m = 0.134$); (b) $Da = 10^{-3}$ ($T_m = 0.048$).

(i) *Effect of Rayleigh number* (*Ra*): The influence of Rayleigh number is shown in Fig. 2 for $Da = 10^{-5}$, $\theta = 45°$, $K^* = 0.1$, $F^* = 10$ and $k^* = 1$ with the variation of *Ra*. It is observed that the flow consists of two cells consisting of clockwise (right) and anti clockwise (left) circulations. As the Rayleigh number increases, the maximum temperature in the cavity (T_m) decreases. The variation of T_m with Darcy number for various Rayleigh numbers is shown in Fig. 3. The decrease in T_m with the increase in *Ra* is due to the increase in vortex strength. It is also observed that the enhanced circulations closer to the cold walls cause strong boundary layer effects on the side walls. It may be noted that T_m always occur at the top edge of the line of symmetry i.e. $x = 0.5$, $y = 1.0$ for isotropic and orthotropic porous medium ($\theta = 0°$ and 90°), but for anisotropic porous medium ($\theta = 45°$) due to higher permeability at an angle of 45° to the vertical axis, the formation of stronger left vortex is observed in Fig. 2. This shifts T_m towards right (0.526, 1) for

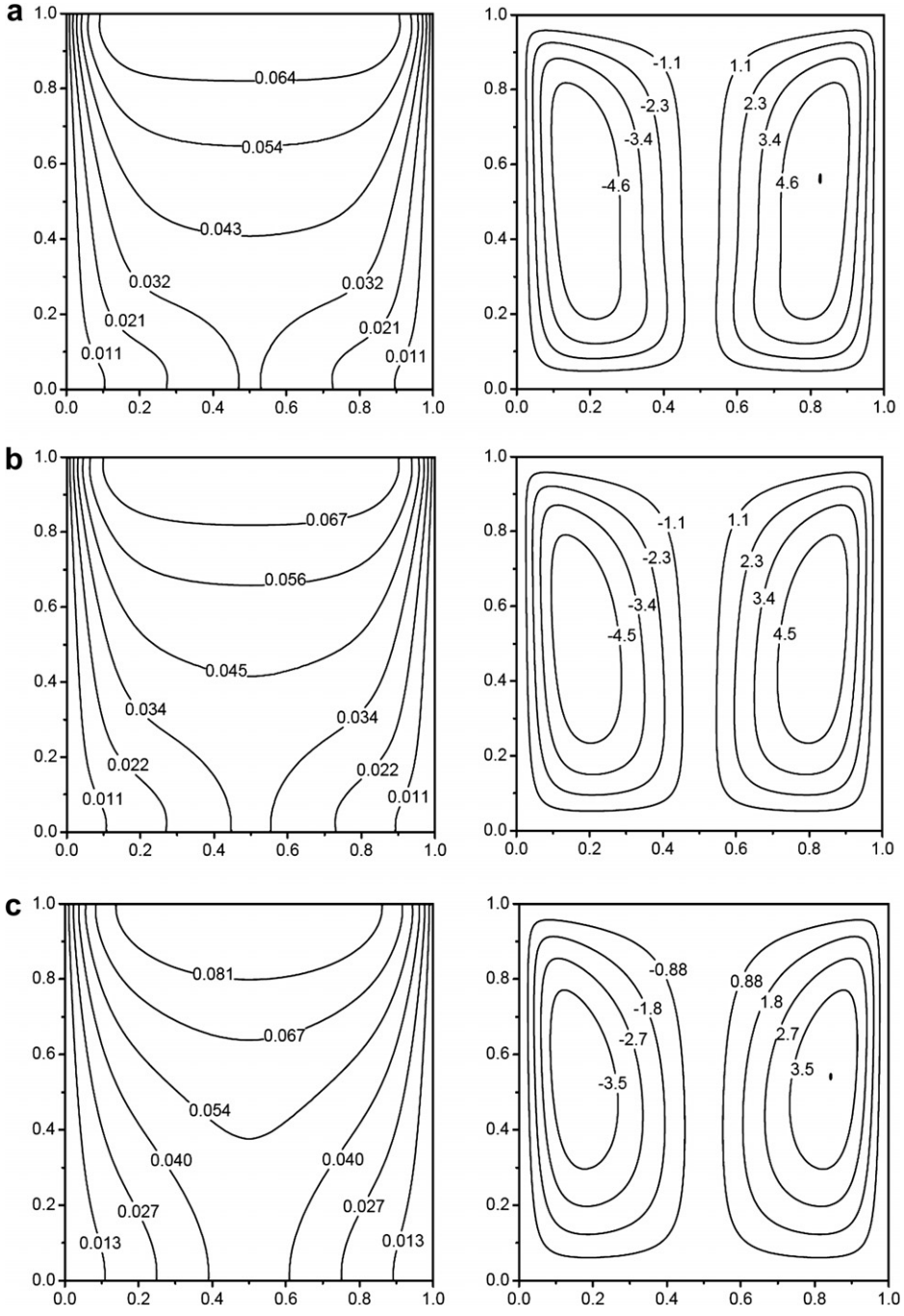

Fig. 5. Isotherms (left) and streamlines (right) for $Ra = 10^7$, $Da = 5 \times 10^{-4}$, $F^* = 1$, $\theta = 90°$ and $k^* = 1$ with the variation of permeability ratio (K^*): (a) $K^* = 0.1$ ($T_m = 0.075$); (b) $K^* = 1$ ($T_m = 0.078$); (c) $K^* = 10$ ($T_m = 0.094$).

$Ra = 10^7$ and (0.679, 1) for $Ra = 10^8$. It is also observed in Fig. 2a for $Ra = 10^7$ the isotherms exhibit minimal distortion, indicating that the conduction is still dominant mechanism of energy transport. However with the increase in Ra, the temperature field is significantly distorted due to higher convective transport. The increase in heat transfer with the increase in Ra is due to the induced temperature gradients between the interstitial fluid and the externally cooled side walls.

(ii) *Effect of Darcy number* (Da): Fig. 4 illustrates isotherms and streamlines for $Ra = 5 \times 10^7$, $\theta = 45°$, $K^* = 0.1$, $F^* = 10$ and $k^* = 1$ for Darcy numbers 10^{-6} and 10^{-3}. For a given set of parameters with the increase in Darcy number, increase in vortex strength is observed due to higher permeability of the porous medium. This leads to increase in convective transport and thus increases energy transport resulting in reduction of T_m. It is observed in Fig. 3 that T_m increases with the decrease of Darcy number. As Darcy number (permeability) is reduced, the obstruction for the flow field increases resulting in reduction of velocity. It is observed in Fig. 4a for a $Da = 10^{-6}$, isotherms exhibit minimal distortion due to lower permeability indicating the energy transport is primarily by conduction. On the other hand, distortion of isotherms may be observed in Fig. 4b due to higher convective transport as higher permeability provides lesser obstruction for the flow field leading to increase in vortex strength. Therefore, T_m increases as Da decreases and vice versa.

(iii) *Effect of permeability ratio* (K^*): Fig. 5 illustrates isotherms and streamlines for $Ra = 10^7$, $Da = 5 \times 10^{-4}$, $\theta = 90°$, $F^* = 1$ and $k^* = 1$ for various K^* varying within 0.1–10. It is observed that the maximum temperature (T_m) increases with the increase in K^*. The increase in K^* progressively weakens the vortex strength due to decrease in permeability in the direction of K_2. Also, the decrease in permeability causes increase in obstruction for the flow field and that retards the flow and decreases convective transport. The isotherm patterns as shown in Fig. 5a–c illustrates that, gradual increase in magnitude of non dimensional temperature is observed with the variation of K^* from 0.1 to 10. The variation of T_m with respect to K^* for various k^* is shown in Fig. 6 for $Ra = 10^7$, $Da = 10^{-4}$, $\theta = 0°$ and $F^* = 1$. It is observed that irrespective of k^*, T_m increases with the increase of K^*. Decreasing trend of T_m with the increase of k^* indicates that the energy transport mechanism is enhanced due to increase in heat transfer by conduction.

(iv) *Effect of inclination of principal axes* (θ): Fig. 7 illustrates the influence of inclination of principal axes (θ) on the variation of T_m with K^* for $Ra = 10^7$, $Da = 10^{-4}$, $F^* = 1$ and $k^* = 1$. It is observed that for $K^* = 0.1$, T_m increases with the increase in θ from 0° to 90°. The permeability is larger in K_2 direction (vertical direction) for $\theta = 0°$ with $K^* = 0.1$ (Eqs. (8), (18)), and as θ increases the permeability decreases in vertical direction. It is observed that the permeability is 10 times less in vertical direction for $\theta = 90°$ when compared to that of $\theta = 0°$ with $K^* = 0.1$. The decrease of permeability in vertical direction with the increase of θ increases the obstruction for the flow field and retards the flow. The reduction of velocity flow field results in decrease of convective transport resulting in increase in T_m. Note that, $K^* = 1$ represents isotropic case which denotes that T_m remains unchanged with respect to θ. For

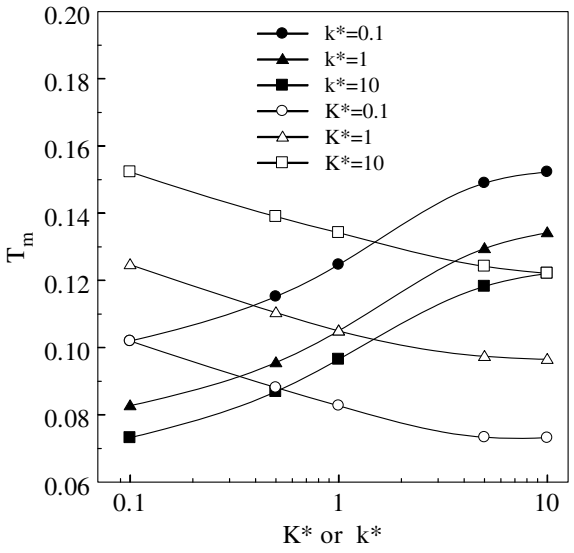

Fig. 6. Effect of permeability ratio (K^*) and thermal conductivity ratio (k^*) on the maximum temperature (T_m) for $Ra = 10^7$, $Da = 10^{-4}$, $\theta = 0°$ and $F^* = 1$.

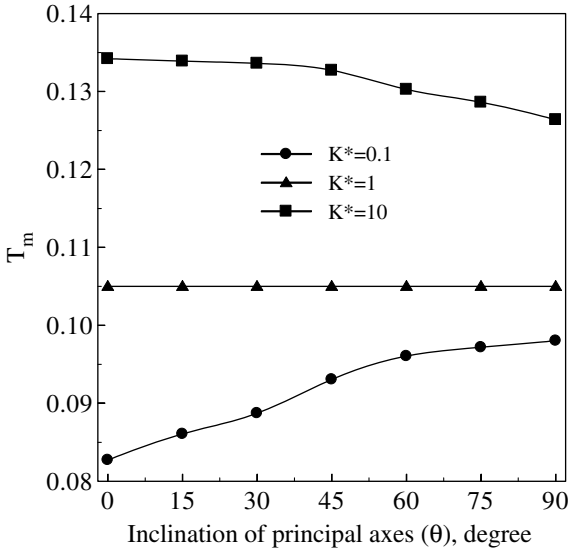

Fig. 7. Effect of inclination of principal axes (θ) on the maximum temperature (T_m) with different permeability ratios (K^*) for $Ra = 10^7$, $Da = 10^{-4}$, $\theta = 0°$ and $F^* = 1$.

$K^* = 10$, a decreasing trend in T_m is observed with the increase of θ from 0° to 90°. For $K^* = 10$ with $\theta = 0°$, the permeability is 10 times less in vertical direction (K_2 direction), when compared to that of horizontal direction (K_1 direction). As θ increases from 0° to 90° with $K^* = 10$ the permeability increases 10 times at an angle θ to the horizontal axis. The increase of permeability in vertical direction with the variation of θ from 0° to 90° leads to increase in energy transport, resulting in decrease of T_m. Fig. 8 illustrates isotherms and streamlines for $Ra = 10^8$, $Da = 10^{-5}$, $K^* = 10$, $F^* = 1$ and $k^* = 10$ with θ ranging within 0–90°. It is observed that the isotherms exhibit minimum distortion as θ varies, indicating that the conduction is the dominant mechanism of heat transfer. As permeability in vertical direction (K_2 direction) is 10 times less than that of horizontal direction (K_1 direction) for $K^* = 10$ with $\theta = 0°$, T_m is larger compared to $\theta > 0°$. For $\theta = 45°$, due to higher permeability (K_1) at an angle of 45° to the ver-

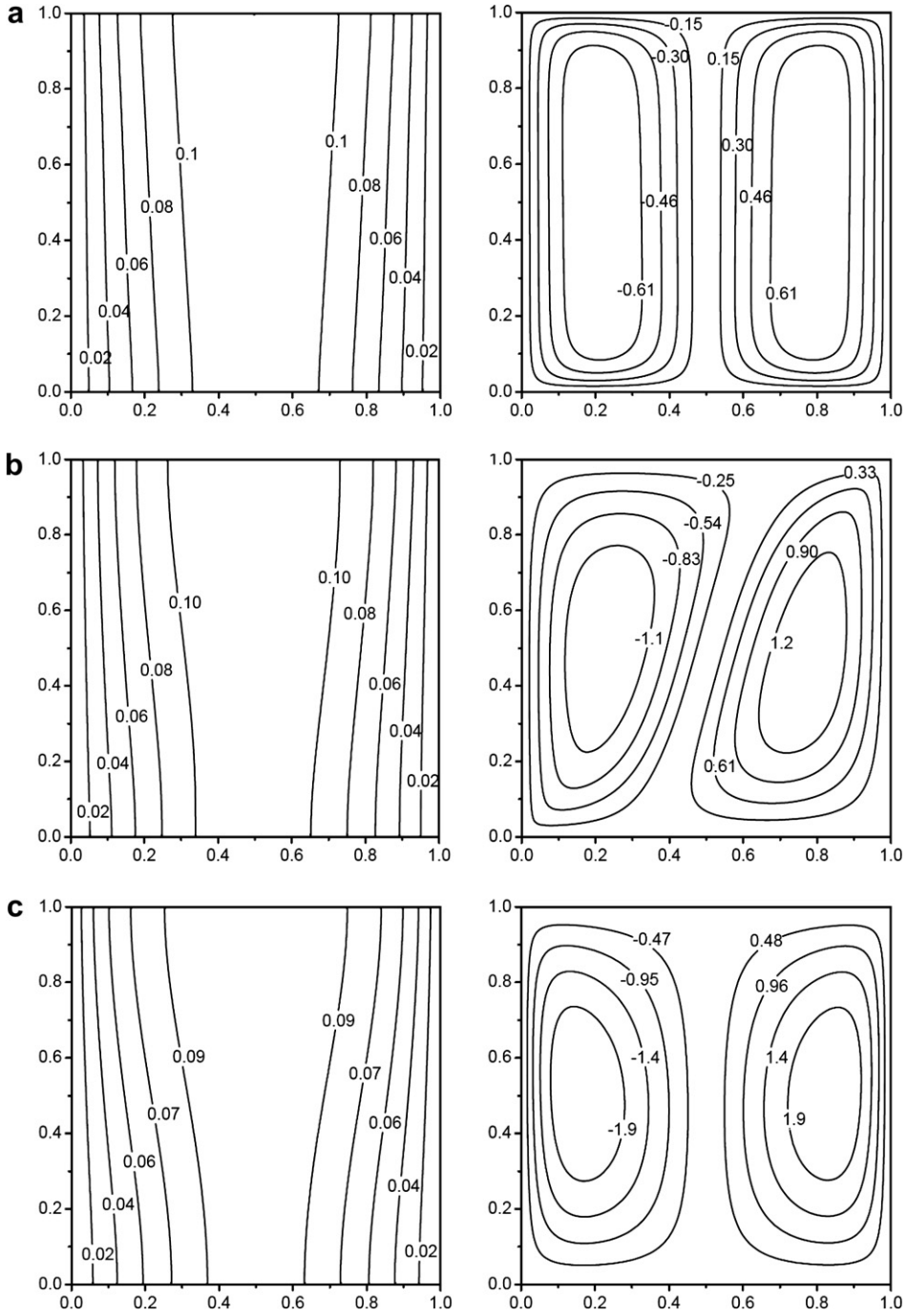

Fig. 8. Isotherms (left) and streamlines (right) for $Ra = 10^8$, $Da = 10^{-5}$, $K^* = 10$, $F^* = 10$ and $k^* = 10$ with the variation of inclination of principal axes (θ): (a) $\theta = 0°$ ($T_m = 0.120$); (b) $\theta = 45°$ ($T_m = 0.117$); (c) $\theta = 90°$ ($T_m = 0.112$).

tical axis the non symmetric nature of the vortices is observed. It is also observed that the vortex strength is larger with $K^* = 10$ for $\theta = 90°$ compared to $\theta = 0°$ due of higher permeability in vertical direction and that results in decrease of T_m.

(v) *Effect of ratio of Forchheimer constants* (F^*): The influence of F^* on T_m with the variation of Da and Ra numbers is shown in Fig. 3 for $K^* = 1$, $\theta = 45°$ and $k^* = 1$. From Eqs. (12), (14) and (18) it can be noted that for $K^* = 1$ the influence of F^* alone can be brought out. It is observed that with the increase in F^*, a decrease in the value of F_2 leads to the reduction of non-linear drag in the direction of F_2 (Fig. 1). As it is well understood that the increase in velocities of the flow field leads to the increase in non-linear drag, evidently the lower velocities of the buoyancy induced flows for the considered range of parameters result in the insignificant nature of F^*

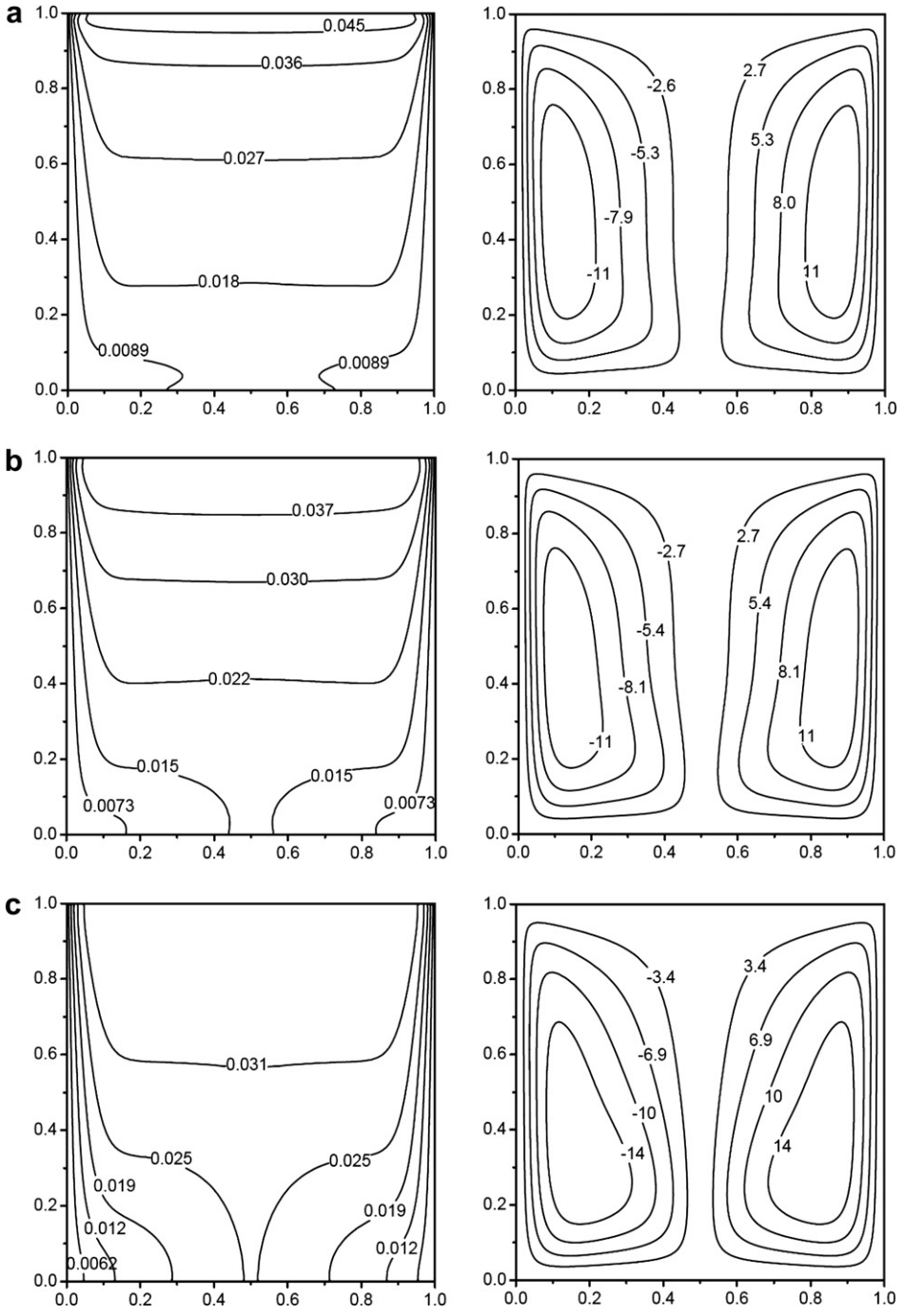

Fig. 9. Isotherms (left) and streamlines (right) for $Ra = 10^8$, $Da = 10^{-3}$, $K^* = 1$, $\theta = 0°$ and $F^* = 1$ with the variation of thermal conductivity ratio (k^*): (a) $k^* = 0.1$ ($T_m = 0.054$); (b) $k^* = 1$ ($T_m = 0.044$); (c) $k^* = 10$ ($T_m = 0.037$).

(vi) *Effect of thermal conductivity ratio* (k^*): Fig. 6 illustrates the variation of T_m with K^* and k^* for $Ra = 10^7$, $Da = 10^{-4}$, $\theta = 0°$ and $F^* = 1$. The maximum temperature (T_m) decreases with the increase in k^* irrespective of K^*. It is observed that T_m follows increased trend with the increase of K^* due to the decrease in permeability. For smaller K^* (higher Darcy numbers) and larger k^*, the heat transport mechanism is dominated both by convective and conduction. Hence, T_m is small compared to remaining simulations shown in Fig. 6. The less distorted nature of isotherms shown in Fig. 8 indicates that, conduction is the dominant mode of heat transfer for larger K^* (low Darcy numbers) and k^* values. Fig. 9 illustrates the isotherms and streamlines for $Ra = 10^8$, $Da = 10^{-3}$, $K^* = 1$, $\theta = 0°$ and $F^* = 1$ for various k^* ranging with in 0.1–10. It may be noted that the thermal conductivity increases in vertical direction as k^* increases. Due to relatively larger thermal conductivity in the vertical direction, the temperature gradients for the interstitial fluid for $k^* = 10$ is smaller than that for $k^* = 0.1$ and 1. The increase in k^* causes a higher flow intensity in the enclosure resulting in reduction of T_m. It is interesting to observe that the isotherms shown in Fig. 8 for $k^* = 10$ is more vertical indicating the heat transport mechanism is dominated by conduction.

(b. i) *Correlation for maximum temperature* (T_m): The maximum temperature (T_m) can be correlated in terms of Rayleigh number (Ra), Darcy number (Da), permeability ratio (K^*), inclination of principal axes (θ), ratio of Forchheimer constants (F^*) and thermal conductivity ratio (k^*) as

$$T_m = 0.631 Ra^{-0.208} Da^{-0.17} (1 + \sin\theta)^{0.084} K^{*0.078} F^{*-0.003} k^{*-0.062}. \quad (30)$$

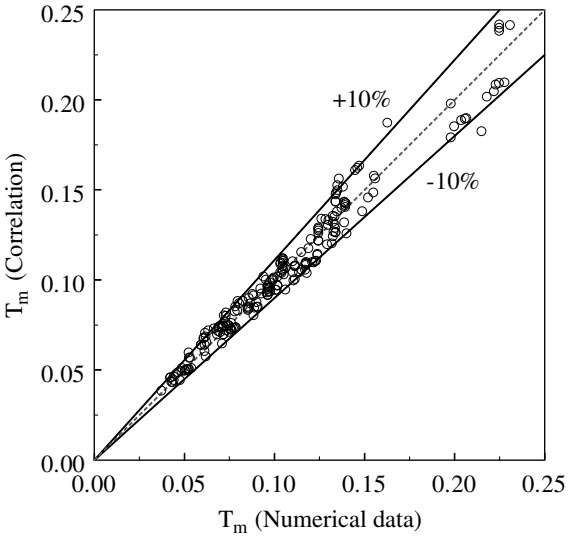

Fig. 10. Parity plot for maximum temperature (T_m).

for the range $10^7 \leqslant Ra \leqslant 10^8$, $10^{-6} \leqslant Da \leqslant 10^{-3}$, $0° \leqslant \theta \leqslant 90°$, $0.1 \leqslant K^* \leqslant 10$, $1 \leqslant F^* \leqslant 100$ and $0.1 \leqslant k^* \leqslant 10$. The power equation (Eq. (30)) is generated by fitting the obtained numerical data through multiple linear regression. To use multiple linear regression, the equation is transformed by taking logarithm (Detailed explanation can be obtained from Ref. [25]). Parity plot with an error of ±10% is shown in Fig. 10. The maximum temperature obtained by using the correlation (Eq. (30)) compares with an average percentage error of 5.21% and with a correlation coefficient of 0.982 to the values obtained by the numerical study.

6. Conclusions

The problem of natural convection in a heat generating anisotropic porous medium is analyzed numerically by generalized non Darcy approach. The present formulation is rigorously validated with the results available in literature. The anisotropic properties considered for the study are permeability ratio (K^*), inclination of principal axes (θ), ratio of Forchheimer constants (F^*) and thermal conductivity ratio (k^*) of the porous medium. The effect of each parameter on the flow and the temperature fields are demonstrated in terms of isotherms, streamlines and maximum temperature. A correlation for maximum temperature in the cavity for $10^7 \leqslant Ra \leqslant 10^8$, $10^{-6} \leqslant Da \leqslant 10^{-3}$, $0° \leqslant \theta \leqslant 90°$, $0.1 \leqslant K^* \leqslant 10$, $1 \leqslant F^* \leqslant 100$ and $0.1 \leqslant k^* \leqslant 10$ has been developed. Based on the parametric study carried out the following conclusive remarks have been obtained:

- As the Rayleigh number increases the maximum temperature in the cavity (T_m) decreases. The increase in heat transfer with the increase in Ra is due to induced density gradients in the interstitial fluid which is due to the generated heat together provided by the cooling at the external walls.
- With the increase in Darcy number (permeability) larger flow velocity is observed. This led to increase in convective transport and thus increases energy transport resulting in decrease of T_m.
- For large permeability ratios ($K^* > 1$) as the anisotropic orientation angle varies from $\theta = 0°$ to 90°, the convective strength of the flow field increases. The heat transport is maximum for $\theta = 90°$ due to higher permeability in vertical direction.
- For small permeability ratios ($K^* < 1$) as the anisotropic orientation angle varies from $\theta = 0°$ to 90°, the convective strength of the flow field gradually diminishes. Due to higher permeability for $\theta = 0°$ in vertical direction the convective transport is maximum.
- The heat transfer mechanism is observed to be more (less) when the porous matrix is oriented in such a way that the principal axes with higher permeability is parallel (perpendicular) to the vertical direction.

- The effect of ratio of Forchheimer constants (F^*) is found to be insignificant for considered range of parameters.
- A large thermal conductivity ratio ($k^* > 1$) causes higher flow intensity in the enclosure. The vertical nature of isotherms for $k^* > 1$ indicates that the heat transfer mechanism to be dominated by conduction. A low thermal conductivity ratio ($k^* < 1$) is observed to have influence on isotherms and streamlines for higher Darcy numbers and found to reduce with the decrease of Darcy number.
- The correlation developed using regression analysis for wide range of parameters gives fairly accurate predictions for the maximum temperature in the cavity. The correlation coefficient and the average percentage error for the correlation are 0.982 and 5.21%, respectively to the values obtained by the numerical study.

References

[1] V. Prasad, Thermal convection in a rectangular cavity filled with a heat generating, Darcy porous medium, ASME J. Heat Transfer 109 (1987) 697–703.

[2] H. Jimenez Islas, F. Lopez-Isunza, J.A. Ochoa-Tapia, Natural convection in a cylindrical porous cavity with internal heat source: A numerical study with Brinkman extended Darcy model, Int. J. Heat Mass Transfer 42 (1999) 4185–4195.

[3] P. Nithiarasu, K.S. Sujatha, K. Ravindran, T. Sundararajan, K.N. Seetharamu, Non-Darcy natural convection in a hydrodynamically and thermally anisotropic porous medium, Comput. Methods Appl. Mech. Eng. 118 (8) (2000) 413–430.

[4] K.J. Beukema, S. Bruin, J. Schenk, Three dimensional natural convection in a confined porous medium with internal heat generation, Int. J. Heat Mass Transfer 26 (1983) 451–458.

[5] M. Haajizadeh, A.F. Ozguc, C.L. Tien, Natural convection in an vertical porous enclosure with internal heat generation, Int. J. Heat Mass Transfer 27 (1984) 1893–1902.

[6] J.J. Royer, L. Flores, Two-dimensional natural convection in an anisotropic and heterogeneous porous medium with internal heat generation, Int. J. Heat Mass Transfer 37 (1994) 1387–1399.

[7] Ch.S.Y. Suresh, T. Sundarajan, S.P. Venkateshan, S.K. Das, Heat transfer from a totally blocked fuel subassembly of a liquid metal fast breeder reactor II. Numerical simulation, Nucl. Eng. Des. 235 (2005) 897–912.

[8] K. Vafai, C.L. Tien, Boundary and inertia effects on flow and heat transfer in porous media, Int. J. Heat Mass Transfer 24 (1981) 195–203.

[9] J. Ettefagh, K. Vafai, S.J. Kim, Non-Darcian effects in open-ended cavities filled with a porous medium, ASME J. Heat Transfer 113 (1991) 747–756.

[10] K. Vafai, S.J. Kim, On the limitation of the Brinkman–Forchheimer-extended Darcy equation, Int. J. Heat Fluid Flow 16 (1995) 11–15.

[11] P. Nithiarasu, K.N. Seetharamu, T. Sundararajan, Natural convective heat transfer in a fluid saturated variable porous medium, Int. J. Heat Mass Transfer 40 (16) (1997) 3955–3967.

[12] M. Anwar Hossain, Mike Wilson, Natural convection flow in a fluid-saturated porous medium enclosed by non-isothermal walls with heat generation, Int. J. Therm. Sci. 41 (2002) 447–454.

[13] T.C. Jue, Analysis of thermal convection in a fluid saturated porous cavity with internal heat generation, J. Heat Mass Transfer 40 (2003) 83–89.

[14] G. Degan, P. Vasseur, E. Bilgen, Convective heat transfer in a vertical anisotropic porous layer, Int. J. Heat Mass Transfer 38 (1995) 1975–1987.

[15] G. Degan, P. Vasseur, Boundary-layer regime in a vertical porous layer with anisotropic permeability and boundary effects, Int. J. Heat Fluid Flow 18 (1) (1997) 334–343.

[16] P. Vasseur, G. Degan, Free convection along a vertical heated plate in a porous medium with anisotropic permeability, Int. J. Numer. Methods Heat Fluid Flow 8 (1) (1998) 43–63.

[17] A. Nakayama, F. Kuwahara, T. Umemoto, T. Hayashi, Heat and fluid flow within an anisotropic porous medium, ASME J. Heat Transfer 124 (2002) 746–753.

[18] A. Nakayama, F. Kuwahara, T. Hayashi, Numerical modelling for three-dimensional heat and fluid flow through a bank of cylinders in yaw, J. Fluid Mech. 498 (2004) 139–159.

[19] S.L. Lee, J.H. Yang, Modeling of Darcy–Forchheimer drag for fluid flow across a bank of circular cylinders, Int. J. Heat Mass Transfer 40 (1997) 3149–3155.

[20] J.H. Yang, S.L. Lee, Effect of anisotropy on transport phenomena in anisotropic porous media, Int. J. Heat Mass Transfer 42 (1999) 2673–2681.

[21] J.C. Ward, Turbulent flow in porous media, in: Proceedings of the American Society of Civil Engineering Journal of Hydraulics Division, No. HY5, vol. 90, 1964, pp. 1–12.

[22] D.A. Nield, A. Bejan, Convection in Porous Media, second ed., Springer, New York, 1999.

[23] J. Ni, C. Beckermann, Natural convection in a vertical enclosure filled with anisotropic porous medium, ASME J. Heat Transfer 113 (1991) 1033–1037.

[24] C. Hirt, A. Amsden, J. Cook, An arbitrary lagrangian Eulerian computing method for all flow speeds, J. Comput. Phys. 14 (1974) 227–253.

[25] S.C. Chapra, R.P. Canale, Numerical Methods for Engineers, fourth ed., Tata McGraw-Hill Edition, New Delhi, 2002.